Regional earthquakes followed by delayed ground uplifts at Campi Flegrei Caldera, Italy

Delayed fluid-driven ground uplift triggered by regional earthquakes at Campi Flegrei Caldera, Italy

Authors: M. Lupi[1,2]*, M. Frehner[2], P. Weis[2,3], E.H. Saenger[2,4], N. Tisato[2,5], S. Geiger[6], G. Chiodini[7], A. Skelton[8], T. Driesner[2]

Affiliations:

1 Department of Earth Sciences, University of Geneva, Switzerland

2 Department of Earth Sciences, ETH Zurich, Switzerland

3 GFZ German Research Centre for Geosciences, Potsdam, Germany

4 International Geothermal Centre, Hochschule Bochum, Bochum, Germany

5 Department of Geological Sciences, Jackson School of Geosciences, The University of Texas at Austin, Austin, TX, USA

6 Institute of Petroleum Engineering, Heriot-Watt University, Edinburgh, Scotland

7 Istituto Nazionale di Geofisica e Vulcanologia, Bologna, Italy

8 Department of Geological Sciences, Stockholm University, Stockholm, Sweden

*Correspondence to: matteo.lupi@unige.ch, thomas.driesner@erdw.ethz.ch

Abstract

Earthquake-triggered volcanic activity promoted by dynamic and static stresses are considered seldom and difficult-to-capture geological processes. Calderas are ideal natural laboratories to investigate earthquake-volcano interactions due to their sensitivity to incoming seismic energy. The Campi Flegrei caldera, Italy, is one of the most monitored volcanic systems worldwide. We compare ground elevation time series at Campi Flegrei with earthquake catalogues showing that uplift events at Campi Flegrei are triggered by large regional earthquakes. Over a 70 years time window we identify 14 uplift events, 12 of them were preceded by an earthquake, and for 8 of them earthquake-to-uplift timespan is within 1.2 yr. To investigate the process that may be responsible for such causative relationship we simulate the propagation of elastic waves and

show that passing body waves impose high dynamic strains at the roof of the magmatic reservoir of the Campi Flegrei at about 7 km depth. This may promote a short-lived embrittlement of the magma reservoir's carapace, which is otherwise impermeable during inter-seismic times. Such failure allows magma and exsolved volatiles to be released from the magmatic reservoir. The fluids, namely exolved volatiles and/or melts, ascent through a nominally plastic zone above the magmatic reservoir. The proposed mechanism and the associated inherent uncertainties require further investigations but the new concept already implies that geological processes triggered by passing seismic waves may become apparent after several months, i.e. far behind the few-days time window normally accepted for dynamic triggering.

1. Introduction

Dynamic stresses associated with passing seismic waves generated by large earthquakes may trigger volcanic activity in the near- and in the far-field within days (Hill et al., 1995, 2002; Linde and Sacks, 1998). It is commonly accepted that surface waves, rather than body waves, are more efficient in promoting earthquake-volcano interactions (Hill and Johnston, 1995; Hill, 2012a; Hill et al., 2002; Husen et al., 2004, 2004; Manga and Brodsky, 2006). However, the proposed models are still difficult to test due to the paucity of recorded triggered events (Prejean and Haney, 2014). As calderas are sensitive to incoming seismic energy (Hill and Johnston, 1995; Husen et al., 2004) they are considered ideal natural laboratories to investigate earthquake-volcano interactions. Some magmatic systems underlying calderas periodically undergo rapid ground uplift phases (Acocella et al., 2015; Chiodini et al., 2012; Hurwitz et al., 2007; Hutnak et al., 2009; Todesco and Berrino, 2005) associated with intense local seismic activity and emission of volcanic gases marked by a strong magmatic component (Bodnar et al., 2007; Chiodini et al., 2012, 2003; Hurwitz et al., 2007; Hutnak et al., 2009; Todesco et al., 2014; Todesco and Berrino, 2005). Uplift phases (known at Campi Flegrei as bradyseismic episodes), generally followed by slow ground deflation (Del Gaudio et al., 2010) are thought to be driven by the rise of hydrothermal fluids or magmas (Battaglia et al., 2006; Bodnar et al., 2007; Chiodini et al., 2003; De Natale et al., 2006).

The Campi Flegrei caldera near Naples, Italy, is characterised by frequent bradyseismic episodes that may reach vertical ground displacement rates of about 1 m/yr (Del Gaudio et al., 2010). Most models relate bradyseismic episodes to the pressurization of the shallow hydrothermal

system by injection of deep fluids (Battaglia et al., 2006; Bodnar et al., 2007; Chiodini et al., 2012; Hurwitz et al., 2007; Hutnak et al., 2009) while others invoke the intrusion of magma at shallow depths (Amoruso et al., 2014; Macedonio, 2014; Woo and Kilburn, 2010). Numerical modelling (Chiodini et al., 2012; Hurwitz et al., 2007; Hutnak et al., 2009; Todesco and Berrino, 2005) in agreement with measured fumarole gas signatures (Chiodini et al., 2012, 2003, 2016a) suggests that CO_2-rich fluids would be particularly efficient in generating the observed uplifts. Previous studies suggest that these fluids are released by a cooling magmatic body at ca. 6–7 km depth (Bodnar et al., 2007; Zollo et al., 2008) and accumulate beneath a low-permeability layer at ca. 3 km depth from which they are then episodically discharged.

In spite of longstanding scientific efforts, a consistent and predictive model accounting for different geological processes at Campi Flegrei is still lacking. By combining analysis of uplift time series, statistical studies and forward simulations of seismic waves, we show evidence for a causal link between regional earthquakes and bradyseismic episodes. We then propose a mechanistic explanation of this link that integrates several of the above-mentioned aspects into a single coherent model. Most notably, our mechanism is compatible with the two scenarios suggesting the release of CO_2-rich brines or the intrusion of magma at shallow depths as the driving force of the bradyseismic episodes.

2. Observations

Since 1905 two distinct phases of ground deformation can be recognised at Campi Flegrei (Del Gaudio et al., 2010; Martino et al., 2014): an overall deflation from 1905 to 1945 (not shown here) recorded by relatively sparse measurements (intervals of several years, refer to Del Gaudio et al., (2010) and Martino et al., (2014) for the entire time sequence), and an overall inflation from 1945 to present (recorded by more frequent measurements after 1980).

SUGGESTED LOCATION OF FIGURE1

To analyse earthquake-volcanoes interactions, namely dynamic triggering (that we define as a measured response of a given geological system caused by external forcing) we analysed inflation and deflation episodes for the period from 1945 to present finding that phases of accelerated uplift may be preceded by large- to middle-size regional earthquakes (Figure 1). This

behaviour is more clear for the major uplift phases starting in 1950 (UL-1), 1967 (UL-3) and 1981 (UL-7). For example, the UL-7 uplift episode (characterised by ca. 1 m/yr uplift rate) started approximately 10 months after the M_w 6.9 Irpinia earthquake in 1980. Also, a more recent and major uplift episode (UL-13) began in early 2010, 11 months after the M_w 6.3 L'Aquila earthquake in 2009 (Figure 1). Non-peer reviewed data seem to suggest that the Campi Flegrei is sensitive to passing seismic waves released by the three most recent regional earthquakes that occurred in Italy in the last decade (i.e., M_w 6.3 L'Aquila in 2009, M_w 6.2 Amatrice in 2016, M_w 6.5 Norcia in 2016). Sansivero et al., (2012) observed marked temperature variations by means of thermal camera at the Solfatara (one of the several craters of the Campi Flegrei) following the M_w 6.3 L'Aquila earthquake (Figure 2a). Furthermore, a report of the Vesuvian Observatory (available at INGV's website) mentions that, *verbatim: "The borehole tilt station ECO recorded a permanent tilt of 0.65 μ in the E direction during the M_w 6.2 Amatrice, Italy, earthquake occurred on the 24th of August 2016 and a tilt of 0.17 μ over 19 mins in the WNW direction during the M_w 6.1 Norcia, Italy, earthquake on the 26th of October 2016",* (INGV October Report, 2016). Additionally, the INGV November Report (2016) shows that the seismic activity increased remarkably immediately after the M_w 6.5 Norcia earthquake on the 30th of October 2016 (Figure 2b).

SUGGESTED LOCATION OF FIGURE2

3. **Data**

Sparse observations are often too descriptive and not rigorous enough to establish a causative relationship between earthquakes and response of the Campi Flegrei to external forcing. To investigate the possible association between earthquakes and bradyseismic episodes we first compared the ground elevation dataset (Del Gaudio et al., 2010; Martino et al., 2014) at Campi Flegrei with earthquake archives (Figure 1c). For the construction of the surface elevation curve of Figure 1c we combined two datasets at the reference point 25A in Campi Flegrei: the first is a reconstruction of the elevation curve from 1945 to 2010 (Del Gaudio et al., 2010); the second is derived from GPS measurements between 2000 and 2015 (Martino et al., 2014). Because the latter has time increment much shorter than the former, we smoothed its short-period oscillations. In particular, we created a common time vector using the 7-days time increment of

the GPS dataset and mapped the elevation dataset onto this common time vector. Finally, from the combined dataset we calculated a 1-year moving average to obtain the 1945 - 2015 elevation curve shown in Figure 1c. We used a 1-year moving average as the focus of our work is on long-term effects. Using a 1-year moving average allowed us to exclude short time-scale oscillations present in the GPS data (Martino et al., 2014).

Next, we compiled a list of all regional earthquakes since 1945 that were larger than M_w 4.5 and closer than 300 km to Campi Flegrei (Figure 1a) and all teleseismic (i.e., worldwide, Figure 1b) earthquakes that were larger than M_w 6.5. To compare the effects of regional and teleseismic earthquakes at Campi Flegrei we calculated the peak ground velocity (PGV) imposed by each of these regional and teleseismic earthquakes at Campi Flegrei as a proxy for their mechanical impact on the caldera. To quantify the predicted PGV we used ground motion prediction equations. For the regional earthquakes we used an equation derived from the Italian strong motion database (Bindi et al., 2011) assuming that the site amplification effect for the reference station inside the Campi Flegrei caldera (40.82750°N, 14.1443°E) is class B (meaning that the shear wave velocities between 0 and 30 m depth range between 360 and 800 m/s). The coefficient Cj is the same for the entire catalogue, i.e., it is assumed as the average value obtained for different frequencies. Finally, we corrected for fault mechanisms for earthquakes from 1979 to 2015 and no focal mechanism was found for the M_w 6.6 earthquake in 1978. However, correction for the focal mechanism does not affect the estimate of PGV for the scope of our work (i.e. it affects the third digit after the comma).

For teleseismic earthquakes we used a similar approach (Agnew and Wyatt, 2014) valid for teleseismic distances (between 500 km and 16000 km) and magnitudes $6.5 \leq M_w \leq 9.0$. The equation estimates the maximum strain (ε) imposed by passing surface waves. As suggested by Manga et al., (2009) we approximate $PGV \simeq \varepsilon \cdot V_s$, with V_s being the shear wave velocity fixed at 2500 m/s for the shallow part of the upper crust. It must be noticed that the equation to estimate the PGV for teleseismic earthquakes was derived for California (Agnew and Wyatt, 2014) and to the best of our knowledge, no regression equation for teleseismic and large-magnitude events has been published for Italy. To obtain realistic PGV results we calibrated V_s until the estimated PGV using the formula of Agnew and Wyatt, (2014) fits the measured PGV values at the reference station to one decimal place. More specifically, we calibrated our estimated PGV

147 values according to measured PGV values imposed by recent major earthquakes (e.g., M_w 9.1
148 Sumatra (2004), M_w 8.8 Maule (2010), M_w 9.0 Tohoku (2011), and M_w 7.1 Van (2011)) recorded
149 at publically accessible INGV seismic stations nearby Campi Flegrei.

150 Our observations rely on the criteria used to determine uplift events. To the best of our
151 knowledge a quantitative description of bradyseismic events does not exist in the literature.
152 Hence, we fit data-driven observations with a quantitative definition of bradyseismic event. Here
153 we define bradyseismic episodes based on two criteria: either i) the uplift rate is larger than 1
154 cm/yr (uplift episodes, shaded grey in Figure 1c) or ii) the uplift rate is 3 cm/yr faster than the
155 average uplift rate of the preceding 3 years (decelerated deflation, shaded yellow in Figure 1c).
156 Based on a qualitative inspection of the data we infer that 12 bradyseismic episodes were
157 preceded by a regional earthquake with an estimated PGV above 0.1 cm/s (see column 3 of
158 Table 1). Only two uplift episodes (UL-4 and UL-12) were not preceded by an earthquake with
159 PGV>0.1 cm/s. The corollary that regional earthquakes with PGV>0.1 cm/s are followed by
160 uplift episodes appears to hold for most of these earthquakes (Table 1).

161 SUGGESTED LOCATION OF TABLE1

162 Before 1980, ground elevation measurements are sparse but still allow us to constrain the onset
163 of uplift episodes. Almost all the earthquakes with PGV>0.1 cm/s during this time period were
164 followed by a ground level measurement, confirming an on-going deflation before the onset of a
165 new uplift episode. The one exception is the M_w 6.1 Irpinia earthquake in 1962. We were unable
166 to verify whether this earthquake was followed by an uplift episode due to the lack of ground
167 elevation measurements.

168

169 **4. Statistical analysis**

170 To assess if the inferred association between earthquakes and bradyseismic episodes is
171 statistically verifiable we carried out a binomial test to investigate the null hypothesis that uplift
172 events are unrelated to earthquakes. To conduct the statistical study we considered regional and
173 teleseismic earthquakes. For the regional earthquakes we had to exclude fore- and after-shocks
174 that may bias the statistical analysis. The excluding criteria for regional earthquakes is shown in
175 Table 1. We define a seismic sequence as the group of seismic events occurring within the

estimated rupture area of the main shock (Wells and Coppersmith, 1994) as either foreshocks (up to two months before the main shock) or aftershocks (up to one year after the main shock). Then we assign the PGV imposed by the main-shock to the seismic sequence and discard the foreshocks and aftershocks in our analysis. This underestimates the total energy reaching the Campi Flegrei caldera. Next, binomial tests were used to compare with the following null hypotheses:

(a) UL/DL onsets occurred randomly and were not related to a previous earthquake.

(b) UL/DL peak uplift rates occurred randomly and were not related to a previous earthquake.

We considered five time windows 0-1 years, 1-2 years, 2-3 years, 3-4 years, and 4-5 years before each uplift/deceleration onset/peak. We use a 1-year time window for this study as we previously used a 1-year moving average to build the surface elevation curve shown in Figure 1c. The probability (p) of an earthquake occurring within these time windows is given by the number of uplift/deceleration events (14) multiplied by the duration of each time window (1 year) divided by the length of the study (70 years). For a 1-year time window, this gives p=0.2, i.e. there is a 20% probability of a random earthquake occurring within one of these pre-defined time windows. The probability (P) that r or more earthquakes with PGV>0.1 cm/s for regional events or PGV>0.01 for teleseismic events occurred during one of these time windows is given by:

$$P = \frac{p^n (1-p)^{(r-n)} r!}{n!(r-n)!}, \quad (1)$$

where n is the total number of earthquakes with PGV>0.1 cm/s (regional events) or PGV>0.01 cm/s (teleseismic events) that occurred during the study. Using the binomial test given by equation (1), we obtained the p-values (P in equation 1) summarized in Figure 3 and given in Table 2.

SUGGESTED LOCATION OF FIGURE3 AND TABLE 2

These values indicate that by using the full catalogue we could reject the null hypothesis (a) for the onset of uplift within one year of a regional earthquake (p-value 0.009) and (b) maximum rate of uplift between 2 and 3 years after the earthquake (p-value 0.049). As mentioned above, aftershock events may bias the statistical analysis favouring a causal relationship between earthquakes and uplift events. However, even with aftershocks removed from the catalogue, we

could still reject the null hypothesis for the onset of uplift occurring within one year of regional earthquakes (p-value 0.007). Using this catalogue we could no longer verify the association between regional earthquakes and the maximum rate of uplift as for the same time delay (2-3 years) we obtain a p-value of 0.3. Null hypothesis (a) cannot be rejected ($p>0.05$) for all other time windows.

For teleseismic earthquakes, all null hypotheses were statistically verified (p-value>0.99), irrespective of the choice of the parameters of the binomial test (e.g., time window and PGV threshold). The test was repeated in reverse, i.e. with the number of time windows given by the number of earthquakes and with n and r given by the total number of uplift events and the number of uplift events that were followed by an earthquake during the assigned time window. This test gave similar results. In this case, we could still reject null hypothesis (a) (but not (b)) for regional earthquakes only. We also varied the PGV thresholds and found that our conclusion holds for PGV<0.22 cm/s for regional earthquakes and that, for teleseismic earthquakes, we cannot reject the null hypothesis regardless of our choice of PGV threshold.

Overall the statistical tests suggest a causal link between bradyseismic episodes and regional earthquakes and indicate that bradyseismic episodes are unrelated to teleseismic earthquakes. We propose that dynamic triggering is the process that is responsible for activating fluid release from the magmatic reservoir underlying the caldera.

5. Numerical Modelling

To identify the possible underlying mechanism for how incoming seismic energy may trigger delayed surface uplift we simulated body wave propagation through the impedance velocity structure of the Campi Flegrei (Vanorio et al., 2005; Zollo et al., 2008). The static model (Figure 4) used for numerical seismic wave propagation modelling is based on an interpreted tomography (Vanorio et al., 2005) and a seismic reflection study (Zollo et al., 2008) and takes into account density variations (Petrillo et al., 2013). The geometry was discretized into a rotated staggered finite-difference grid of 2.5×10^7 nodes with a grid spacing of 0.675 m. We used periodic boundary conditions on the sides of the model domain and a free surface at the top of the domain.

SUGGESTED LOCATION OF FIGURE4

The amplitude of the incoming synthetic wave is constrained such that the average vertical displacement at the surface in the simulations matches the amplitude of the recorded seismic wave that we used to calibrate the simulations. We simulate body and surface waves. P- and Love waves have weaker effects compared to S- and Rayleigh waves, respectively, and are not shown here. For body waves we assumed a central frequency of 1 Hz and for surface waves a central period of 20 s. This was because Hill (2012b) shows that surface waves with central periods around 20 s may be particularly effective in pumping fluids out of magmatic reservoirs. Because the frequency of the simulated body wave is 1 Hz, we can assume that the resulting maximum absolute strain value on a specific component of the strain tensor obtained from our simulations may translate directly to strain rate values. The numerical code used in this study (Saenger et al., 2000) assumes an elastic domain. The full procedure, from discretization to model calibration is described in Lupi et al. (2013). To construct the numerical model we simplified the magmatic reservoir as an elliptical magma chamber. We calibrated the model with observed frequency contents and ground displacements caused by several earthquakes for both regional and teleseismic events. Maximum strains (Figure 5a) generated by incident shear waves at 1 Hz (central frequency) reach 10^{-5} while energy densities (Figure 5b) are in the order of 1 J/m^3. Seismic wave simulations using lower central frequencies (i.e., 0.5 Hz) yield lower but still significant values (i.e., maximum strains of 10^{-6}).

SUGGESTED LOCATION OF FIGURE5

Simulations of Rayleigh waves with a central period of 20 s highlight that surface waves impose remarkably weaker shear strains compared to shear waves at Campi Flegrei on the deep magmatic reservoir (i.e., three orders of magnitude less) (Figure 6). Elevated strain rates and maximum energy densities focus in regions characterized by large seismic impedance contrasts, such as the interface between the deep magmatic reservoir and the host rocks. This coincides with regions of inferred breaching of low permeability zones (Bodnar et al., 2007) (i.e., at ca. 3 km depth and at the top of the magma reservoir at ca. 7 km depth). According to our simulations, energy density appears to be more effectively captured when seismic waves travel from a low to a high shear wave velocity body and not vice versa. Hence, direct body waves released from regional earthquakes crossing the magma-host rock impedance contrast from below, rather than

surface waves generated by teleseismic events penetrating the system from surface to depth, seem to be more effective in focusing dynamic strains at the interface between the magmatic reservoir and the host rock. This is in agreement with our statistical analysis as at short epicentral distances (i.e., for regional earthquakes) PGV is principally caused by body waves (Kulhánek, 2002).

SUGGESTED LOCATION OF FIGURE6

6. Discussion

The ground at calderas undergoing bradyseism is constantly in motion with either uplift or deflation dominating the temporal evolution. Continuous monitoring allows identification of single uplift events of highly variable magnitudes, but the precise timing of onset and peak uplift is naturally blurred by the superposition of events and can only be approximated by identifying acceleration and deceleration of ground motion. Typically, the bradyseismic events indicate a delay time of about one to three years between onset and peak of uplift, followed by a longer period of deflation. A conceptual mechanistic model therefore not only has to provide a plausible explanation for the trigger but also for the intrinsic year-long timescales of ground motion and its natural variability.

In line with the variability of the delay time, our statistical analysis indicates that the relationship between regional earthquakes and onset of uplift is stronger than the relationship between regional earthquakes and peak of uplift. We further test if larger earthquakes trigger faster uplifts by plotting the peak uplift rate against PGV of all earthquake-uplift event-couples (red dots in Figure 7), which suggests a positive correlation for the regional earthquakes, but no correlation for teleseismic earthquakes (blue dots in Figure 7). Even though data is sparse and the correlation may be dominated by a prominent earthquake-uplift couple (i.e the M6.9 Irpinia) the plot further supports a causal relationship between regional (and not teleseismic) earthquakes and uplift events.

SUGGESTED LOCATION OF FIGURE7

The results of the numerical simulations indicate that the incoming seismic energy from regional earthquakes has the strongest effects at the base of the shallow hydrothermal system and at the roof of the magma chamber. The wave-induced short-lived dynamic strain rates localized at

approximately 7 km depth (Figure 5) can temporarily induce embrittlement in regions of otherwise hot ductile rocks around the magma chamber. The ductile yield curve can be approximated (Fournier, 1999) as:

$$\dot{\epsilon}=A(\sigma_1-\sigma_3)^n \exp[-Q/(RT)], \quad (2)$$

where $\dot{\epsilon}$ is strain rate, R the universal gas constant, $\sigma_1-\sigma_3$ the differential stress affecting the media, T temperature, n the stress exponent, and Q (activation energy) and A coefficients representing the type of lithology. As A, n, Q, R, and T are constant at a given point in the system, the passing wave induces increased strain rates and higher differential stresses ($\sigma_1-\sigma_3$) shifting the ductile yield curve to greater depths (Figure 8a). This creates a short-lived (co-seismic) brittle region (red region in Figure 8b) within the otherwise ductile domain. The resulting failure taps the reservoir of accumulated magmatic fluids (Figure 8c). Note that we do not discuss static stress triggering in our manuscript because static stress triggering operates at the fault length scale (Toda et al., 2011). Although static Coulomb stresses cannot be ruled out for the 1980 M6.9 Irpinia earthquake, we propose that static stress variations imposed by 11 out of 12 earthquakes do not impose significant stress variations at Campi Flegrei because the epicentral distance from Campi Flegrei is too large.

Earlier conceptual models (Fournier, 1999) and more recent numerical simulations for ore-forming magmatic-hydrothermal systems (Weis et al., 2012) suggest that the released magmatic fluids can rapidly ascend through a hot, nominally ductile region with lithostatic fluid pressure above the magmatic reservoir. The timescale of the vertical ascent of overpressured fluids from the magma reservoir depends on the amount of permeability increase due to hydraulic fracturing, which is not trivial to constrain. Numerical modelling of fluid release in porphyry copper systems suggest that permeability increase and flow rates depend on the amount of overpressured fluids, which in turn depends on the release rate from the magma chamber, attaining velocities in the order of km/yr (Weis et al., 2012). The numerical model further suggests that once the fluids are released, they will continue ascending as pulses of overpressured fluids invoking upward-moving permeability-creating fracturing events. Permeability estimates in response to major earthquakes indicate that even higher flow rates can be temporarily obtained in even deeper crustal levels (Ingebritsen, 2012). The inferred process of fluid ascent will naturally also depend on the state of the magmatic system, in particular on the availability of fluids during the seismic

triggering event. On the other hand, events of fluid release may also be caused by the evolution of the magmatic system itself and therefore do not require an external trigger (Fournier, 1999). The inferred process would therefore also be consistent with missing earthquake-uplift couples and variable onset-to-peak delay times.

Supercritical H_2O-CO_2 mixtures with compositions observed at Campi Flegrei fumaroles (Chiodini et al., 2003, 2012, 2016) will remain at near constant density of ca. 0.5 g/cm^3 during ascent through the lithostatically pressured region. The time lags identified in this study approximately represent the time necessary for the fluids to migrate from the magmatic reservoir to the top of the ductile region at Campi Flegrei located at approximately 3 km depth (Petrillo et al., 2013). There, a strong expansion is caused by phase separation of the H_2O-CO_2 fluid mixture under hydrostatic conditions (Figure 8c).

SUGGESTED LOCATION OF FIGURE8

The phase separation can efficiently impose significant uplifts as shown in previous studies (Chiodini et al., 2012; Hutnak et al., 2009; Todesco and Berrino, 2005) and, once fluid pressure is dissipated, the ground may subside again (Todesco et al., 2014). Our proposed mechanism is in agreement with numerical models suggesting that deflation periods follow episodic fluid fluxes, possibly in conjunction with permeability and/or porosity changes due to hydraulic fracturing, fracture sealing and/or compaction of the porous medium in relation to fluid-driven pressure variations (Chiodini et al., 2012; Hutnak et al., 2009; Todesco et al., 2014; Todesco and Berrino, 2005). The onset of uplift may be less affected than the peak of uplift by shallow processes that are activated by the upwelling fluids once they enter hydrothermal system (e.g., reactivation of different fault systems, variations of permeability, slow versus fast thermal expansion), which could explain the differences in statistical relevance.

At Campi Flegrei, long-term deflation periods (e.g., 1985-2005) are suggested to be associated with compaction of the porous media driven by fluid pressure drops in the order of 1 MPa (Todesco et al., 2014). In line with these models, our proposed mechanism infers that the onset of the deflation phase occurs when the fluid pressure induced by the expansion of the H_2O-CO_2 fluid mixture, which drives the uplift phase, is relaxed. This is due to a reduced provision of fluids from depth and the contemporaneous fluid release from the shallow hydrothermal system

(which increases from approximately 3400 ton/day during deflation periods to approximately 12000 ton/day during uplift events (Todesco and Berrino, 2005).

Our model is also in agreement with recent findings (Chiodini et al., 2016b) pointing out that magmatic volatiles released by magmatic bodies in a near-critical-state (i.e., the magmatic reservoir at 7 km depth beneath Campi Flegrei) can cause volcanic unrest. The Campi Flegrei is a system capable of retaining near-critical conditions in the shallow hydrothermal systems, and possibly at greater depths, thanks to the geotechnical properties of the shallow lithologies capable of withstanding elevated strain rates (Vanorio and Kanitpanyacharoen, 2015).

Our study points out that processes activated by passing seismic waves may become apparent long after the time span of few days commonly accepted for dynamic triggering. Although for Campi Flegrei we notice that 8 out of 12 uplift events began within 1.2 yr from the triggering earthquake, the earthquake-uplift time lag may vary. We argue that such variable time window exists because the proposed process of fluid release and ascent is influenced by several first-order controls such as rate of fluid exsolution from the magma, CO_2 content of the upwelling fluids, and amount of permeability increase during fluid ascent. Additionally, volcanic systems are geological environments with non-linear behavior undergoing inflation and deflation phases, implying that the preparedness of the volcanic system may vary over time. Vargas et al., (2017) show how the physical state of the hydrothermal and magmatic system of the Nevados del Ruiz, Colombia, changed over 20 years. The Campi Flegrei may have undergone similar variations over the last 70 years resulting in a continuous variation of the physical state of its hydrothermal and magmatic system, and hence its preparedness to dynamic triggering. This may play a key role in explaining the time-variations in the response timespans shown in Table 1 (and in Figure S1 in the supplemental material). The comparatively low occurrence of large magnitude regional earthquakes hampers the strength of statistical correlation, which is not favored by the two different types of dataset that we cross-correlate. However, the strong qualitative observations and the quantitative analysis (in particular for the post-1990 period) strongly support the temporal relationship between seismic events and maximum vertical uplift rates.

This manuscript proposes a provocative idea relating earthquakes and uplift events. Further studies will be needed for verification and quantification of the proposed model, which has the potential to become a valuable observation for risk mitigation plans. More generally, if our

proposed model is correct, the timescales of uplift could provide natural evidence reflecting fluid flow processes in magmatic-hydrothermal systems.

Conclusions

We show that the Campi Flegrei is sensitive to incoming seismic energy, i.e. body waves, released by regional earthquakes. Other calderas undergo similar phases of inflation and deflation, with some of them also be proven to be sensitive to incoming seismic energy. The time lags proposed in our study suggest that processes activated by dynamic triggering may become apparent long after the commonly accepted timespan of a few days. This introduces the concept of delayed dynamic triggering. Although examples of short-timing volcanic triggering (i.e. within a few days) are becoming more and more frequent such examples are still limited. However, disturbance of the magmatic systems, not necessarily directly causing immediate eruptions, could be a much more widespread process. Our work shows that potentially triggered changes can be manifested on timescales of several months.

ACKNOWLEDGMENTS:

Donat Fäh is thanked for suggesting the ground motion classification of the earthquakes. Nima Riahi, Jean-Pierre Burg, and Stephen A. Miller for discussion of the paper. Matteo Lupi thanks SCCER-SoE and the Swiss National Science Foundation for financial support (grant n° PZ00P2_154815 and grant n° PYAPP2_166900).

References

Acocella, V., Di Lorenzo, R., Newhall, C., Scandone, R., 2015. An overview of recent (1988 to 2014) caldera unrest: Knowledge and perspectives. Rev. Geophys. 53, 896–955. doi:10.1002/2015RG000492

Agnew, D.C., Wyatt, F.K., 2014. Dynamic Strains at Regional and Teleseismic Distances. Bull. Seismol. Soc. Am. 104, 1846–1859. doi:10.1785/0120140007

Amoruso, A., Crescentini, L., Sabbetta, I., De Martino, P., Obrizzo, F., Tammaro, U., 2014. Clues to the cause of the 2011-2013 Campi Flegrei caldera unrest, Italy, from continuous GPS data. Geophys. Res. Lett. 41, n/a-n/a. doi:10.1002/2014GL059539

Battaglia, M., Troise, C., Obrizzo, F., Pingue, F., De Natale, G., 2006. Evidence for fluid migration as the source of deformation at Campi Flegrei caldera (Italy). Geophys. Res. Lett. 33.

Bindi, D., Pacor, F., Luzi, L., Puglia, R., Massa, M., Ameri, G., Paolucci, R., 2011. Ground motion prediction equations derived from the Italian strong motion database. Bull. Earthq. Eng. 9, 1899–1920. doi:10.1007/s10518-011-9313-z

417 Bodnar, R.J., Cannatelli, C., De Vivo, B., Lima, A., Belkin, H.E., Milia, A., 2007. Quantitative model for magma
418 degassing and ground deformation (bradyseism) at Campi Flegrei, Italy: Implications for future eruptions.
419 Geology. doi:10.1130/G23653A.1
420 Chiodini, G., Caliro, S., De Martino, P., Avino, R., Gherardi, F., 2012. Early signals of new volcanic unrest at
421 Campi Flegrei caldera? Insights from geochemical data and physical simulations. Geology 40, 943–946.
422 doi:10.1130/G33251.1
423 Chiodini, G., Paonita, A., Aiuppa, A., Costa, A., Caliro, S., De Martino, P., Acocella, V., Vandemeulebrouck, J.,
424 Aiuppa, A., Patanè, D., Gori, P. De, Chiarabba, C., Bonaccorso, A., Poland, M.P., Miklius, A., Sutton, A.J.,
425 Thornber, C.R., Sigmundsson, F., Sigmundsson, F., Sparks, R.S.J., Tilling, R.I., Voight, B.R., Cornelius, R.R.,
426 Chiodini, G., Caliro, S., Martino, P. De, Avino, R., Gherardi, F., Chiodini, G., Sheridan, M.F., Wohletz, K.H.,
427 Acocella, V., Lorenzo, R. Di, Newhall, C., Scandone, R., Costa, A., Gaudio, C. Del, Aquino, I., Ricciardi,
428 G.P., Ricco, C., Scandone, R., D'Auria, L., Caliro, S., Chiodini, G., Paonita, A., D'Auria, L., Linde, A.T.,
429 Sacks, I.S., Pallister, J.S., Hoblitt, R.P., Reyes, A.G., Papale, P., Moretti, R., Barbato, D., Tilling, R.I., Blundy,
430 J., Cashman, K. V., Rust, A., Witham, F., Hurwitz, S., Lowenstern, J.B., Burgisser, A., Alletti, M., Scaillet,
431 B., Dixon, J.E., Marziano, G.I., Morizet, Y., Trong, E. Le, Gaillard, F., Liu, Y., Zhang, Y., Behrens, H.,
432 Newman, S., Lowenstern, J.B., Chiodini, G., Zollo, A., Stock, M.J., Humphreys, M.C.S., Smith, V.C., Isaia,
433 R., Pyle, D.M., Aiuppa, A., Paonita, A., Caracausi, A., Iacono-Marziano, G., Martelli, M., Rizzo, A., Tassi, F.,
434 Nicholson, E.J., Mather, T.A., Pyle, D.M., Odbert, H.M., Christopher, T., Cartwright, J., Hansen, D.M.,
435 Dawson, P., Whilldin, D., Chouet, B., Paulatto, M., Minshull, T.A., Henstock, T.J., Preston, R.J., Menand, T.,
436 Phillips, J.C., Woods, A.W., Cardoso, S.S.S., Caliro, S., Chiodini, G., Marini, L., Luccio, F. Di, Pino, N.A.,
437 Piscini, A., Ventura, G., Dusseault, M.B., Collins, P.M., Dusseault, M.B., Heap, M.J., Baud, P., Meredith,
438 P.G., Vinciguerra, S., Reuschlé, T., Heap, M.J., Segall, P., Bell, A.F., Naylor, M., Heap, M.J., Main, I.G.,
439 Vasseur, J., Voight, B.R., Chang, W.L., Smith, R.B., Farrell, J., Puskas, C.M., Martino, P. De, Tammaro, U.,
440 Obrizo, F., Afanasyev, A.A., Afanasyev, A.A., Afanasyev, A., Costa, A., Chiodini, G., Chiodini, G., Todesco,
441 M., Chiodini, G., Macedonio, G., Todesco, M., Todesco, M., Rutqvist, J., Chiodini, G., Pruess, K., Oldenburg,
442 C.M., Chiodini, G., 2016a. Magmas near the critical degassing pressure drive volcanic unrest towards a
443 critical state. Nat. Commun. 7, 13712. doi:10.1038/ncomms13712
444 Chiodini, G., Paonita, A., Aiuppa, A., Costa, A., Caliro, S., De Martino, P., Acocella, V., Vandemeulebrouck, J.,
445 Aiuppa, A., Patanè, D., Gori, P. De, Chiarabba, C., Bonaccorso, A., Poland, M.P., Miklius, A., Sutton, A.J.,
446 Thornber, C.R., Sigmundsson, F., Sigmundsson, F., Sparks, R.S.J., Tilling, R.I., Voight, B.R., Cornelius, R.R.,
447 Chiodini, G., Caliro, S., Martino, P. De, Avino, R., Gherardi, F., Chiodini, G., Sheridan, M.F., Wohletz, K.H.,
448 Acocella, V., Lorenzo, R. Di, Newhall, C., Scandone, R., Costa, A., Gaudio, C. Del, Aquino, I., Ricciardi,
449 G.P., Ricco, C., Scandone, R., D'Auria, L., Caliro, S., Chiodini, G., Paonita, A., D'Auria, L., Linde, A.T.,
450 Sacks, I.S., Pallister, J.S., Hoblitt, R.P., Reyes, A.G., Papale, P., Moretti, R., Barbato, D., Tilling, R.I., Blundy,
451 J., Cashman, K. V., Rust, A., Witham, F., Hurwitz, S., Lowenstern, J.B., Burgisser, A., Alletti, M., Scaillet,
452 B., Dixon, J.E., Marziano, G.I., Morizet, Y., Trong, E. Le, Gaillard, F., Liu, Y., Zhang, Y., Behrens, H.,
453 Newman, S., Lowenstern, J.B., Chiodini, G., Zollo, A., Stock, M.J., Humphreys, M.C.S., Smith, V.C., Isaia,
454 R., Pyle, D.M., Aiuppa, A., Paonita, A., Caracausi, A., Iacono-Marziano, G., Martelli, M., Rizzo, A., Tassi, F.,
455 Nicholson, E.J., Mather, T.A., Pyle, D.M., Odbert, H.M., Christopher, T., Cartwright, J., Hansen, D.M.,
456 Dawson, P., Whilldin, D., Chouet, B., Paulatto, M., Minshull, T.A., Henstock, T.J., Preston, R.J., Menand, T.,
457 Phillips, J.C., Woods, A.W., Cardoso, S.S.S., Caliro, S., Chiodini, G., Marini, L., Luccio, F. Di, Pino, N.A.,
458 Piscini, A., Ventura, G., Dusseault, M.B., Collins, P.M., Dusseault, M.B., Heap, M.J., Baud, P., Meredith,
459 P.G., Vinciguerra, S., Reuschlé, T., Heap, M.J., Segall, P., Bell, A.F., Naylor, M., Heap, M.J., Main, I.G.,
460 Vasseur, J., Voight, B.R., Chang, W.L., Smith, R.B., Farrell, J., Puskas, C.M., Martino, P. De, Tammaro, U.,
461 Obrizo, F., Afanasyev, A.A., Afanasyev, A.A., Afanasyev, A., Costa, A., Chiodini, G., Chiodini, G., Todesco,
462 M., Chiodini, G., Macedonio, G., Todesco, M., Todesco, M., Rutqvist, J., Chiodini, G., Pruess, K., Oldenburg,
463 C.M., Chiodini, G., 2016b. Magmas near the critical degassing pressure drive volcanic unrest towards a
464 critical state. Nat. Commun. 7, 13712. doi:10.1038/ncomms13712
465 Chiodini, G., Todesco, M., Caliro, S., Del Gaudio, C., Macedonio, G., Russo, M., 2003. Magma degassing as a
466 trigger of bradyseismic events: The case of Phlegrean Fields (Italy). Geophys. Res. Lett. 30.
467 De Natale, G., Troise, C., Pingue, F., Mastrolorenzo, G., Pappalardo, L., Battaglia, M., Boschi, E., 2006. The Campi
468 Flegrei caldera: unrest mechanisms and hazards. Geol. Soc. London, Spec. Publ. 269, 25–45.
469 Del Gaudio, C., Aquino, I., Ricciardi, G.P., Ricco, C., Scandone, R., 2010. Unrest episodes at Campi Flegrei: A
470 reconstruction of vertical ground movements during 1905–2009. J. Volcanol. Geotherm. Res. 195, 48–56.
471 EMSC website [WWW Document], n.d. URL http://www.emsc-csem.org/Earthquake/?filter=yes
472 Fournier, R.O., 1999. Hydrothermal processes related to movement of fluid from plastic into brittle rock in the

magmatic-epithermal environment. Econ. Geol. 94, 1193–1211. doi:10.2113/gsecongeo.94.8.1193
Hill, D.P., Johnston, M., 1995. Response of Long Valley caldera to the Mw= 7.3 Landers, California, earthquake. J. Geophys. ….
Hill, D.P., Johnston, M., Langbein, J., Bilham, R., 1995. Response of Long Valley Caldera to the M=7.3 Landers, California, Earthquake. Geophys. Res. Lett. 100, 12985–13005.
Hill, D.P., 2012a. Surface-wave potential for triggering tectonic (nonvolcanic) tremor-corrected. Bull. Seismol. Soc. Am. 102, 2337–2355. doi:10.1785/0120120086
Hill, D.P., Pollitz, F., Newhall, C., 2002. Earthquake–Volcano Interactions. Phys. Today 55, 41. doi:10.1063/1.1535006
Hurwitz, S., Christiansen, L.B., Hsieh, P.A., 2007. Hydrothermal fluid flow and deformation in large calderas : Inferences from numerical simulations. J. Geophys. Res. 112.
Husen, S., Taylor, R., Smith, R.B., Healser, H., 2004. Changes in geyser eruption behavior and remotely triggered seismicity in Yellowstone National Park produced by the 2002 M 7.9 Denali fault earthquake, Alaska. Geology 32, 537–540.
Husen, S., Taylor, R., Smith, R.B., Healser, H., 2004. Changes in geyser eruption behavior and remotely triggered seismicity in Yellowstone National Park produced by the 2002 M 7.9 Denali fault earthquake, Alaska. Geology 32, 537. doi:10.1130/G20381.1
Husen, S., Wiemer, S., Smith, R.B., 2004. Remotely triggered seismicity in the Yellowstone National Park region by the 2002 Mw 7.9 Denali Fault earthquake, Alaska. Bull. Seismol. Soc. Am. 94, S317--S331.
Hutnak, M., Hurwitz, S., Ingebritsen, S.E., Hsieh, P.A., 2009. Numerical models of caldera deformation: Effects of multiphase and multicomponent hydrothermal fluid flow. J. Geophys. Res. 114, B04411. doi:10.1029/2008JB006151
INGV, n.d. No Title [WWW Document]. URL http://www.ov.ingv.it/ov/en/campi-flegrei/275.html
INGV-Nov.Report, 2016. No Title [WWW Document]. URL http://www.ov.ingv.it/ov/bollettini-mensili-campania/Bollettino_Vulcani_Campani_2016_11.pdf
INGV-Oct.Report, 2016. No Title.
Kulhánek, O., 2002. 21 The structure and interpretation of seismograms. Int. Geophys. 81, 333–348.
Linde, A.T., Sacks, I.S., 1998. Triggering of volcanic eruptions. Nature 395, 888–890.
Lupi, M., Saenger, E.H., Fuchs, F., Miller, S.A., 2013. Lusi mud eruption triggered by geometric focusing of seismic waves. Nat. Geosci. 6, 642–646.
Macedonio, G., 2014. Sill intrusion as a source mechanism of unrest at volcanic calderas. … Res. Solid Earth.
Manga, M., Brodsky, E., 2006. Seismic triggering of eruptions in the far field: Volcanoes and geysers. Annu. Rev. Earth Planet. Sci 34, 263–291.
Manga, M., Brumm, M., Rudolph, M.L., 2009. Earthquake triggering of mud volcanoes. Mar. Pet. Geol. 26, 1785–1798. doi:10.1016/j.marpetgeo.2009.01.019
Martino, P. De, Tammaro, U., Obrizzo, F., 2014. GPS time series at Campi Flegrei caldera (2000-2013). Ann. Geophys. 57. doi:10.4401/ag-6431
Mele, F., Marcocci, C., Moro, R., 2007. ISIDe, Italian Seismic Instrumental and parametric Data base [WWW Document]. URL http://iside.rm.ingv.it (accessed 5.30.16).
Petrillo, Z., Chiodini, G., Mangiacapra, A., Caliro, S., Capuano, P., Russo, G., Cardellini, C., Avino, R., 2013. Defining a 3D physical model for the hydrothermal circulation at Campi Flegrei caldera (Italy). J. Volcanol. Geotherm. Res.
Prejean, S.G., Haney, M.M., 2014. Geophysics. Shaking up volcanoes. Science 345, 39. doi:10.1126/science.1256196
Saenger, E.H., Gold, N., Shapiro, S.A., 2000. Modeling the propagation of elastic waves using a modified finite-difference grid. Wave motion 31, 77–92.
Sansivero, F., Vilardo, G., De Martino, P., Augusti, V., Chiodini, G., 2012. Campi Flegrei volcanic surveillance by thermal IR continuous monitoring, in: 11th International Conference on Quantitative InfraRed Thermography. Department of Aerospace Engineering University of Naples Federico II.
Toda, S., Stein, R.S., Sevilgen, V., Lin, J., 2011. Coulomb 3. 3 Graphic-rich deformation and stress-change software for earthquake, tectonic, and volcano research and teaching-user guide.
Todesco, M., Berrino, G., 2005. Modeling hydrothermal fluid circulation and gravity signals at the Phlegraean Fields caldera. Earth Planet. Sci. Lett. 240, 328–338.
Todesco, M., Costa, A., Comastri, A., Colleoni, F., Spada, G., Quareni, F., 2014. Vertical ground displacement at Campi Flegrei (Italy) in the fifth century: Rapid subsidence driven by pore pressure drop. Geophys. Res. Lett. 41, 1471–1478. doi:10.1002/2013GL059083

USGS [WWW Document], n.d. URL https://earthquake.usgs.gov/earthquakes/search/

Vanorio, T., Kanitpanyacharoen, W., 2015. Rock physics of fibrous rocks akin to Roman concrete explains uplifts at Campi Flegrei Caldera. Science (80-.). 349.

Vanorio, T., Virieux, J., Zollo, A., Capuano, P., Russo, G., de Nice, U. e, di Napoli, U. a, 2005. 3-D Seismic Tomography from P-and S-Microearthquake Traveltimes and Rock Physics Characterization in the Campi Flegrei Caldera. J. Geophys. Res 110, B03201.

Vargas, C.A., Koulakov, I., Jaupart, C., Gladkov, V., Gomez, E., El Khrepy, S., Al-Arifi, N., 2017. Breathing of the Nevado del Ruiz volcano reservoir, Colombia, inferred from repeated seismic tomography. Sci. Rep. 7, 46094. doi:10.1038/srep46094

Weis, P., Driesner, T., Heinrich, C.A., 2012. Porphyry-copper ore shells form at stable pressure-temperature fronts within dynamic fluid plumes. Science 338, 1613–6. doi:10.1126/science.1225009

Wells, D.L., Coppersmith, K.J., 1994. New empirical relationships among magnitude, rupture length, rupture width, rupture area, and surface displacement. Bull. Seismol. Soc. Am. 84, 974–1002.

Woo, J.Y.L., Kilburn, C.R.J., 2010. Intrusion and deformation at Campi Flegrei, southern Italy: Sills, dikes, and regional extension. J. Geophys. Res. Solid Earth 115, 1–21. doi:10.1029/2009JB006913

Zollo, A., Maercklin, N., Vassallo, M., Dello Iacono, D., Virieux, J., Gasparini, P., 2008. Seismic reflections reveal a massive melt layer feeding Campi Flegrei caldera. Geophys. Res. Lett. doi:10.1029/2008GL034242

FIGURES AND TABLES

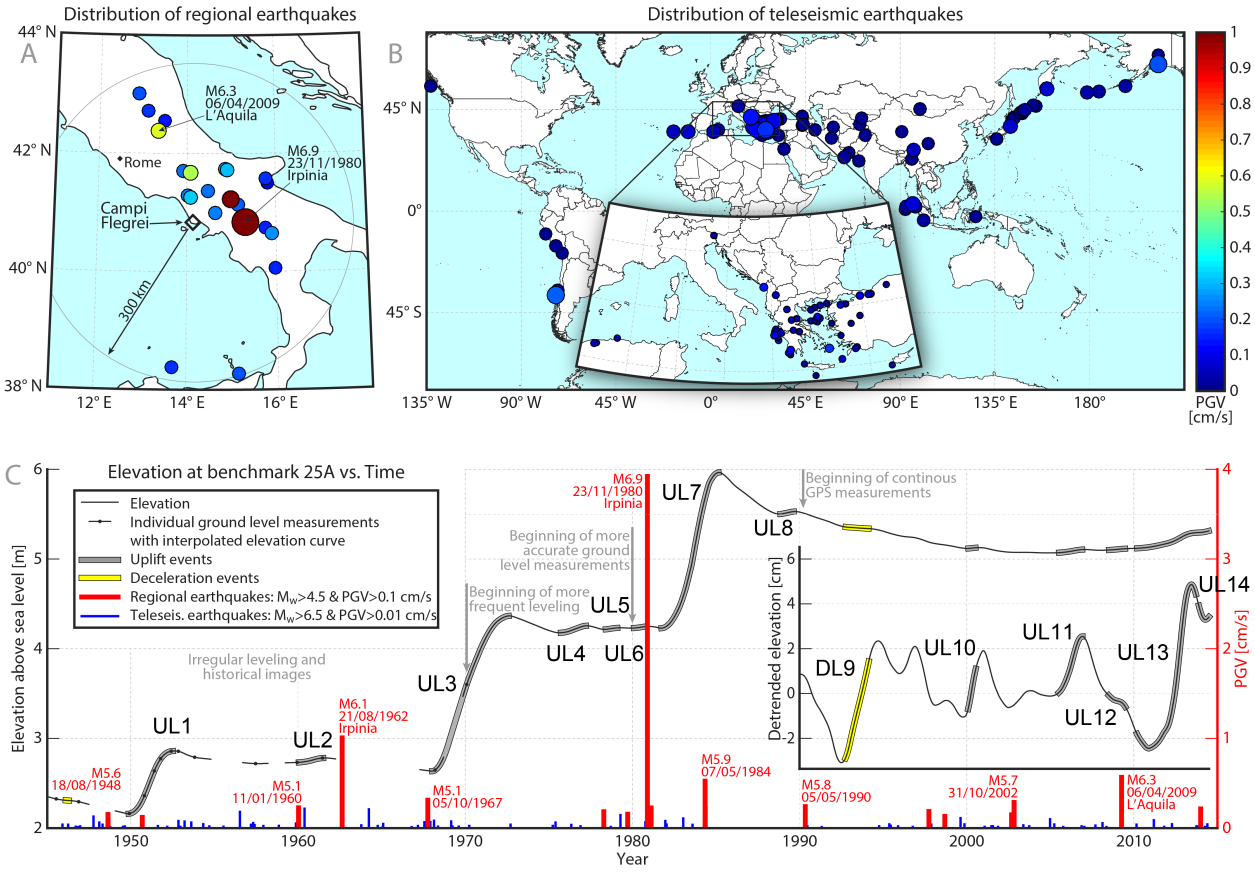

Figure 1. Earthquake catalogue and uplift data used in the study. A) Geographic distribution of regional and B) teleseismic earthquakes. Color-coding refers to imposed PGV at Campi Flegrei. C) One-year moving average of the ground elevation measured at the reference point 25A at Campi Flegrei and time distribution of earthquakes from 1945 to present (adapted from Del Gaudio et al., 2010 and De Martino et al., 2014). The height of the bars represents the calculated PGV at Campi Flegrei. The inset in C shows the elevation curve for the 1990 to present period de-trended using the best-fitting sine curve. The earthquake dataset is publically available and can be retrieved from the Italian earthquake catalogue from 1945 to 2006 (Mele et al., 2007) and from the EMSC website from 2006 to present for the regional earthquakes and from the cached version of the USGS earthquake archive for the teleseismic earthquakes from 1945 to 2015.

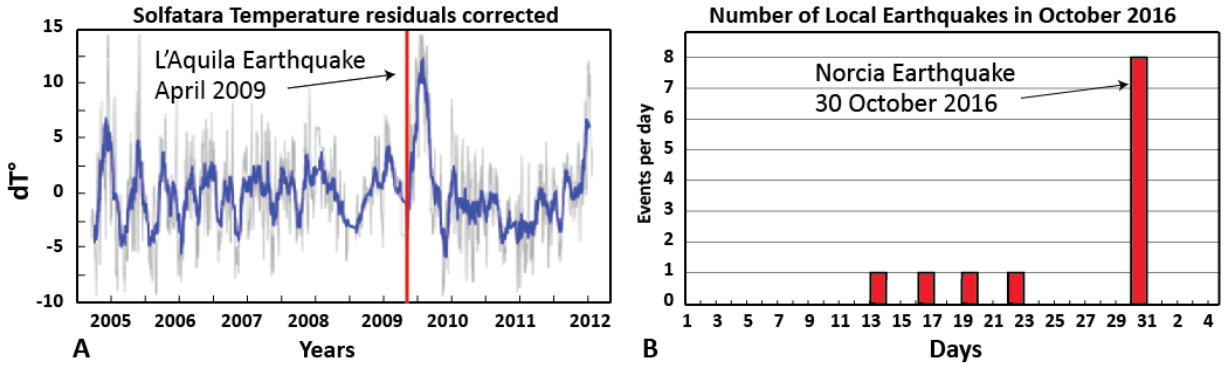

Figure 2. Effects of regional earthquakes at Campi Flegrei. A) Chronograms of the maximum InfraRed temperature variations of the whole scene of the Solfatara after temperature residuals seasonal cyclicity removal - sky excluded (modified after Sansivero et al., 2012) Note the sharp peak after the M_w 6.3 L'Aquila earthquake. B) Number of local seismic events recorded at Campi Flegrei during October 2016. Note the increase on the 30th of October 2016, the day of the M_w 6.5 Norcia earthquake.

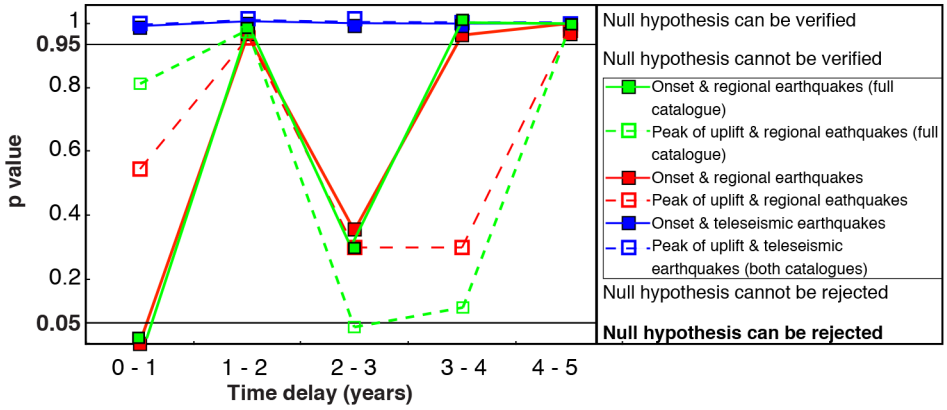

Figure 3. Statistical study. The null hypothesis for the onset of uplift events could be rejected for the 0-1 year time period for both catalogues (see text). Note that in binomial tests it is possible to set any arbitrary time window to try to capture all earthquake/uplift pairs. However, the binomial test has a build-in penalty for doing so: if the time window is longer, the p-value will increase accordingly. The null hypothesis for the peak of uplift events could be rejected for the 2-3 years time period for the full catalogue and for the 2.3-3.8 years period (not shown here) for the catalogue of Table 2. The null hypotheses for teleseismic earthquakes were all verified.

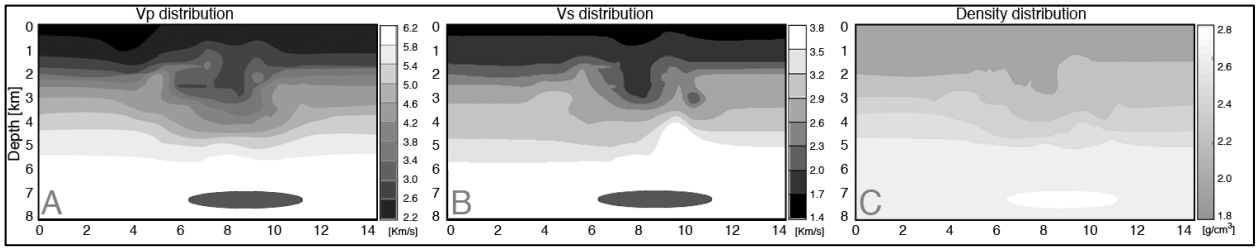

Figure 4. Velocity and density structure of the Campi Flegrei caldera. Both the P- and S-wave velocity structure (including the magma properties) are reconstructed from tomography and seismic reflection studies of the Campi Flegrei (Vanorio et al., 2005; Zollo et al., 2008). Density variations are taken from Petrillo et al. (2013). The velocity model measures 14x8 km and represents a E-W profile across the caldera.

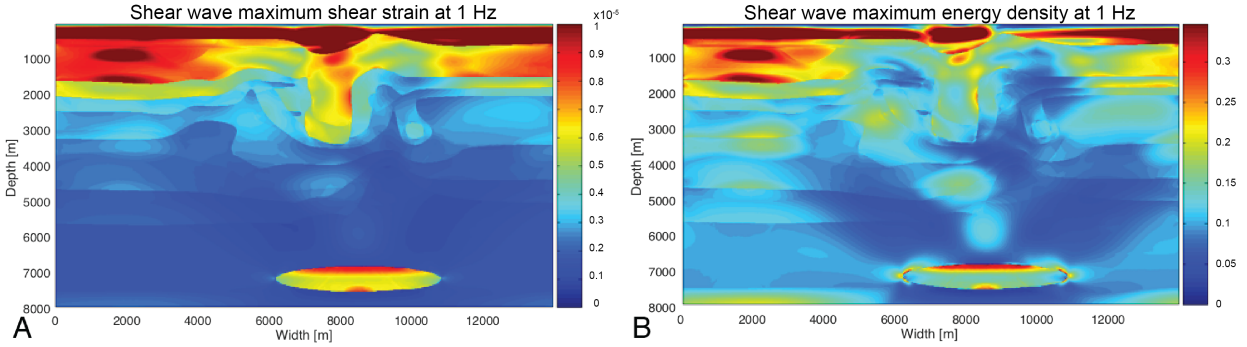

Figure 5. Simulation results at 1 Hz for S-waves. Results are calibrated with the seismic record of the L'Aquila earthquake for 1 Hz frequency at the INGV seismic station OVO (coordinates 40.82750°N, 14.39667°E). Note that maximum values are reached at shallow depths, in the central part of the model (i.e., at 3 km depth), and at the interface between the magma chamber and the overlying host rocks.

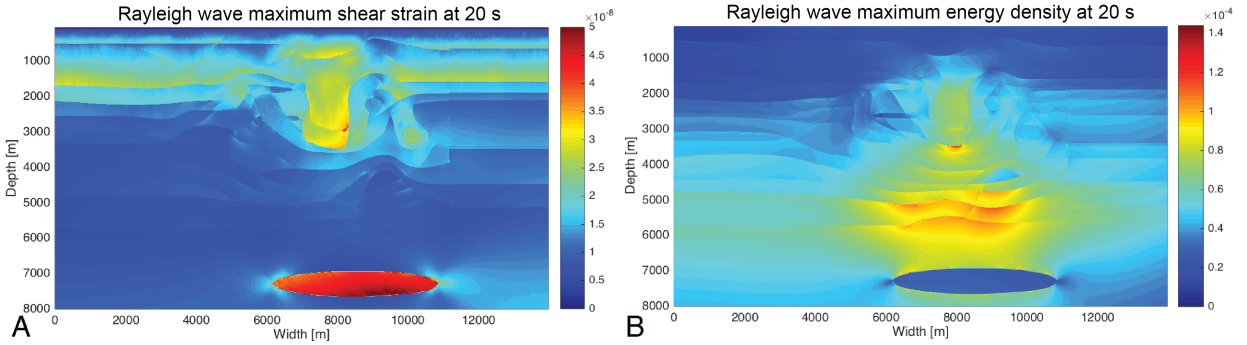

Figure 6. Effects of Rayleigh waves with a period of 20 s at Campi Flegrei. Note that compared to Figure 5 the values of shear strain and energy density for surface waves are three and four orders of magnitude smaller, respectively.

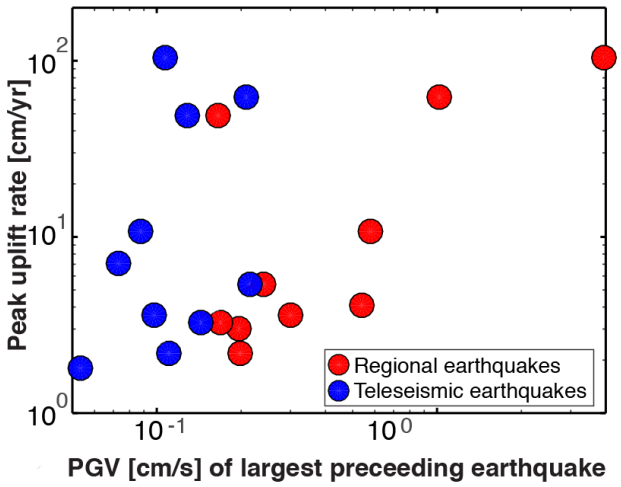

Figure 7. Linear relationship between calculated PGV and peak uplift rate. Larger PGV promote faster uplifts for regional earthquakes. No correlation could be found for teleseismic earthquakes. The he R^2 value for a possible fitting line would be R^2=0.47 ($\log_{10}$(peak uplift rate [cm/yr])=0.97*$\log_{10}$(PGV [cm/s])+1.37) The fitting is clearly dominated by the M_w 6.9 earthquake. However, when removing this event the linear correlation still appears.

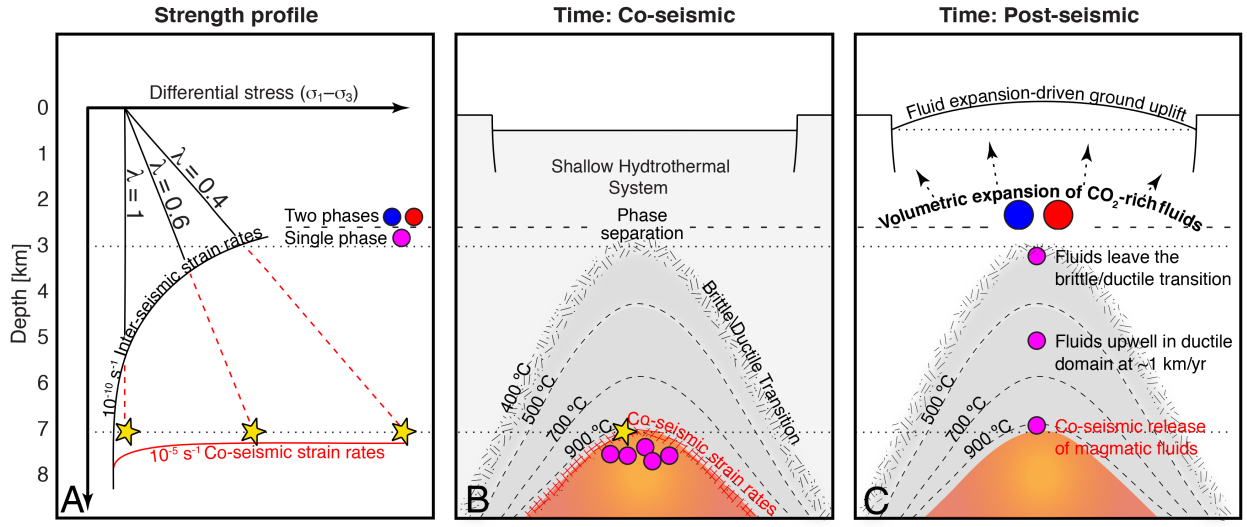

Figure 8. Conceptual model illustrating the effects of large earthquakes at the Campi Flegrei caldera. A) Strength-vs.-depth profile for various fluid factors (λ). λ is the ratio between pore fluid pressure and overburden stress. The intersection between the brittle yield curve (diagonal lines) and the ductile yield curve (curved lines) marks the brittle/ductile transition. Inter- and co-seismic times are marked in black and red, respectively. The incoming seismic waves impose local and temporarily high strain rates of ca. 10^{-5} s^{-1}. Yellow stars indicate regions of embrittlement for different λ. B) Localization of high strains at the roof of the magma chamber promotes the release of single-phase magmatic fluids (purple circles) that subsequently flow through the ductile domain maintaining a quasi-constant volume. C) Upwelling fluids undergo phase separation (red and blue circles) and volumetric expansion at the base of the hydrothermal system.

Table 1. Summary of major regional events of our catalogue in relation to bradyseismic episodes. Grey bars indicate each uplift period and show the beginning, the peak, and the end of the period. M_w is the moment magnitude and FM is the focal mechanism, where N, SS, R, and U, stand for normal, strike slip, reverse, and unknown, respectively. UL stands for uplift and DL for deceleration. The first panel of the table considers all the events with $_{PGV}$ greater than 0.1 cm/s that can be retrieved from the catalogues. Seismic events are progressively excluded from the first and second panel to obtain the third panel of the table that shows the seismic events (i.e., the main shocks) used to conduct the statistical study. The color coding indicates the criteria used to exclude the seismic event.

ALL REGIONAL EARTHQUAKES WITH PGV>0.1				
All Regional events PGV>0.1 + Aftershocks				
EQ ranked on PGV	Date	M_w	Dist	PGV
EQ 20	1948.633	5.6	157.83	0.17
EQ 32	1948.641	5.4	157.48	0.11
UL1 - 1949.816 - 1951.080 - 1952.518				
EQ 30	1950.302	4.4	41.68	0.12
EQ 27	1950.680	5.6	199.5	0.13
EQ 12	1960.030	5.0	52.36	0.24
UL2 - 1960.050 - 1960.931 - 1961.506				
EQ 2	1962.641	6.1	81.27	1.02
EQ 5	1962.641	5.7	80.06	0.48
EQ 16	1962.641	5.4	88.44	0.21
EQ 6	1967.764	5.1	47.43	0.32
EQ 7	1968.041	6.3	355.8	0.31
UL3 - 1968.052 - 1969.000 1972.603				
UL4 - 1975.458 - 1976.359 - 1977.221				
EQ 11	1976.350	6.4	607.5	0.24
EQ 18	1978.291	6.1	296.4	0.20
UL5 - 1978.401 - 1978.620 - 1979.100				
EQ 19	1979.719	5.8	227.8	0.17
UL6 - 1980.096 - 1980.537 - 1980.844				
EQ 1	1980.896	6.9	95.81	3.93
EQ 33	1980.899	5.1	94.58	0.10
EQ 21	1980.902	5.4	111.8	0.17
EQ 29	1981.044	5.2	109.1	0.12
EQ 13	1981.122	4.9	43.96	0.24
UL7 - 1981.744 - 1983.642 - 1985.155				
EQ 4	1984.352	5.9	93.63	0.54
EQ 15	1984.363	5.5	100.2	0.23
UL8 - 1988.854 - 1989.391 - 1989.909				
EQ 10	1990.347	5.8	147.6	0.25
EQ 24	1990.347	5.5	134.8	0.14
DL9 - 1992.764 - 1994.106 - 1994.106				
EQ 17	1997.738	6.0	265.5	0.20
EQ 25	1998.691	5.6	174.9	0.14
UL10 - 1999.9701- 2000.296 - 2000.583				
EQ 23	1999.775	3.8	20.05	0.16
EQ 22	2002.683	5.9	275.2	0.16
EQ 8	2002.835	5.7	116.9	0.30
EQ 9	2002.836	5.7	117.1	0.29
EQ 26	2005.391	4.4	36.07	0.14
UL11 - 2005.528 - 2006.333 - 2006.908				
UL12 - 2008.518 - 2008.9978 - 2009.476				
EQ 3	2009.266	6.3	185.7	0.58
EQ 28	2009.269	5.6	175.0	0.13
UL13 - 2010.204 - 2012.792 - 2013.692				
EQ 31	2012.388	6.1	510.8	0.11
EQ 14	2013.996	5.2	65.54	0.23
UL14 - 2014.0082				

ALL (AFTERSHOCKS AND PGV VALUES NOT CORRECTED FOR FOCAL MECHANISMS)				
Regional events with PGV>0.1 Cleaned for M_w and Dist				
EQ ranked o PGV	Date	M_w	Dist	PGV
EQ 20	1948.633	5.6	157.83	0.17
EQ 32	1948.641	5.4	157.48	0.11
UL1 - 1949.816 - 1951.080 - 1952.518				
EQ 27	1950.680	5.6	199.53	0.13
EQ 12	1960.030	5.0	52.36	0.24
UL2 - 1960.050 - 1960.931 - 1961.506				
EQ 2	1962.641	6.1	81.27	1.02
EQ 5	1962.641	5.7	80.06	0.48
EQ 16	1962.641	5.3	88.44	0.21
EQ 6	1967.764	5.1	47.43	0.32
UL3 - 1968.052 - 1969.000 1972.603				
UL4 - 1975.458 - 1976.359 - 1977.221				
EQ 18	1978.291	6.1	296.45	0.20
UL5 - 1978.401 - 1978.620 - 1979.100				
EQ 19	1979.719	5.8	227.80	0.17
UL6 - 1980.096 - 1980.537 - 1980.844				
EQ 1	1980.896	6.9	95.81	3.93
EQ 33	1980.899	5.1	94.58	0.10
EQ 21	1980.902	5.4	111.83	0.17
EQ 29	1981.044	5.2	109.10	0.12
EQ 13	1981.122	4.9	43.96	0.24
UL7 - 1981.744 - 1983.642 - 1985.155				
EQ 4	1984.352	5.9	93.63	0.54
EQ 15	1984.363	5.5	100.21	0.23
UL8 - 1988.854 - 1989.391 - 1989.909				
EQ 10	1990.347	5.8	147.66	0.25
EQ 24	1990.347	5.5	134.81	0.14
DL9 - 1992.764 - 1994.106 - 1994.106				
EQ 17	1997.738	6.0	265.56	0.20
EQ 25	1998.691	5.6	174.94	0.14
UL10 - 1999.9701- 2000.296 - 2000.583				
EQ 22	2002.683	5.9	275.26	0.16
EQ 8	2002.835	5.7	116.94	0.30
EQ 9	2002.836	5.7	117.16	0.29
UL11 - 2005.528 - 2006.333 - 2006.908				
UL12 - 2008.518 - 2008.9978 - 2009.476				
EQ 3	2009.266	6.3	185.74	0.58
EQ 28	2009.269	5.6	175.05	0.13
UL13 - 2010.204 - 2012.792 - 2013.692				
EQ 14	2013.996	5.2	65.54	0.23
UL14 - 2014.0082				

EARTHQUAKES USED IN THE STATISTICAL STUDY				
Regional events with PGV>0.1 cleaned for M_w and Dist and No Aftershocks, after correction for focal mechanisms				
EQ ranked on PGV	Date	M_w	Dist	PGV – corrected
EQ 20-U	1948.633	5.6	157.83	0.17
UL1 - 1949.816 - 1951.080 - 1952.518				
EQ 27-U	1950.680	5.6	199.53	0.13
EQ 12-U	1960.030	5.0	52.36	0.24
UL2 - 1960.050 - 1960.931 - 1961.506				
EQ 2-U	1962.641	6.1	81.27	1.02
EQ 6-U	1967.764	5.1	47.43	0.32
UL3 - 1968.052 - 1969.000 1972.603				
UL4 - 1975.458 - 1976.359 - 1977.221				
EQ 18-U	1978.291	6.1	296.45	0.20
UL5 - 1978.401 - 1978.620 - 1979.100				
EQ 19-N	1979.719	5.8 6	227.80	0.17
UL6 - 1980.096 - 1980.537 - 1980.844				
EQ 1-N	1980.896	6.9	95.81	3.93
EQ 13-N	1981.122	4.9	43.96	0.24
UL7 - 1981.744 - 1983.642 - 1985.155				
EQ 4-N	1984.352	5.9	93.63	0.54
UL8 - 1988.854 - 1989.391 - 1989.909				
EQ 10-SS	1990.347	5.8	147.66	0.25
DL9 - 1992.764 - 1994.106 - 1994.106				
EQ 17-N	1997.738	6.0	265.56	0.20
UL10 - 1999.9701- 2000.296 - 2000.583				
EQ 22-SS	2002.683	5.9	275.26	0.16
EQ 8-SS	2002.835	5.7	116.94	0.30
UL11 - 2005.528 - 2006.333 - 2006.908				
UL12 - 2008.518 - 2008.9978 - 2009.476				
EQ 3-N	2009.266	6.3	185.74	0.58
UL13 - 2010.204 - 2012.792 - 2013.692				
EQ 14-N	2013.996	5.2	65.54	0.23
UL14 - 2014.008 - still ongoing				

Removed because:	
	Below M_w4.5
	Further than 300 km threshold
	Aftershock of same seismic sequence (kept the one with larger PGV)
	Removed after fault correction - below 0.1 PGV cm/s

Table 2. Results of statistical analysis. The null hypothesis can be verified for all cases except for those that are underlined. The null hypothesis can be rejected for the case in bold text and underlined.

Binomial Test (no Aftershock considered, only the earthquakes in Table 1)					
	0 -1 yr	1-2 yr	2-3 yr	3-4 yr	4-5 yr
Onset (R-EQ)	**0.007**	0.97	0.40	1	0.97
Peak (R-EQ)	0.55	0.95	0.30	0.30	1
Onset (T-EQ)	1.0	1.0	1.0	1.0	1.0
Peak (T-EQ)	1.0	1.0	1.0	1.0	1.0
Binomial Test (Full catalogue)					
	0 -1 yr	1-2 yr	2-3 yr	3-4 yr	4-5 yr
Onset (R-EQ)	**0.009**	0.97	0.34	1.0	1.0
Peak (R-EQ)	0.83	0.99	**0.049**	0.12	1.0
Onset (T-EQ)	1.0	1.0	1.0	1.0	1.0
Peak (T-EQ)	1.0	1.0	1.0	1.0	1.0

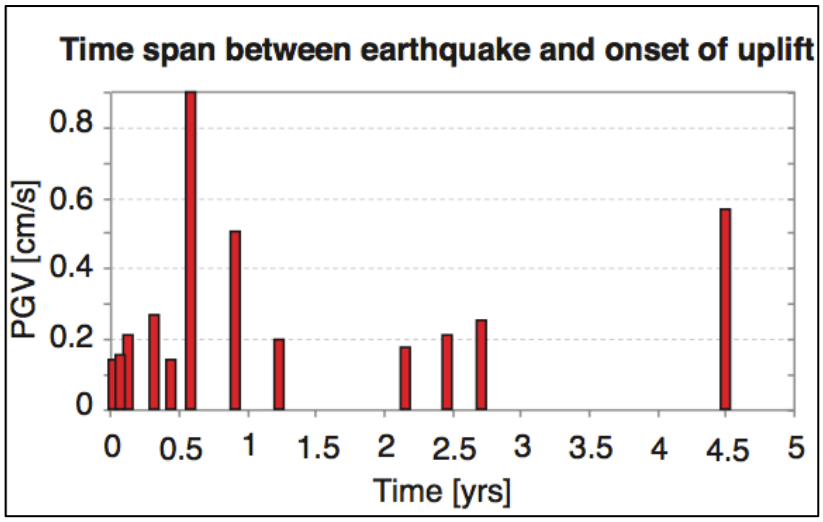

Figure S1. Delay between earthquakes and onset of uplift. Note that 8 out of 12 earthquakes occur within approximately 1.2 yrs before the onset of uplift.